Remote Sens. **2014**, *6*, 1684-1704; doi:10.3390/rs6021684

OPEN ACCESS

remote sensing

ISSN 2072-4292

www.mdpi.com/journal/remotesensing

Article

A Comparative Analysis of EO-1 Hyperion, Quickbird and Landsat TM Imagery for Fuel Type Mapping of a Typical Mediterranean Landscape

Giorgos Mallinis [1,*], Georgia Galidaki [2] and Ioannis Gitas [2]

[1] Department of Forestry and Management of the Environment and Natural Resources, School of Agricultural Sciences and Forestry, Democritus University of Thrace, Orestiada 68200, Greece

[2] Forestry and Natural Environment, School of Agriculture, Aristotle University of Thessaloniki, Thessaloniki 54124, Greece; E-Mails: galidaki@for.auth.gr (G.G.); igitas@for.auth.gr (I.G.)

***** Author to whom correspondence should be addressed; E-Mail: gmallin@fmenr.duth.gr; Tel.: +30-2552-041-107; Fax: +30-2552-041-192.

Received: 31 December 2013; in revised form: 8 February 2014 / Accepted: 13 February 2014 / Published: 20 February 2014

Abstract: Forest fires constitute a natural disturbance factor and an agent of environmental change with local to global impacts on Earth's processes and functions. Accurate knowledge of forest fuel extent and properties can be an effective component for assessing the impacts of possible future wildfires on ecosystem services. Our study aims to evaluate and compare the spectral and spatial information inherent in the EO-1 Hyperion, Quickbird and Landsat TM imagery. The analysis was based on a support vector machine classification approach in order to discriminate and map Mediterranean fuel types. The fuel classification scheme followed a site-specific fuel model within the study area, which is suitable for fire behavior prediction and spatial simulation. The overall accuracy of the Quickbird-based fuel type mapping was higher than 74% with a quantity disagreement of 9% and an allocation disagreement of 17%. Both classifications from the Hyperion and Landsat TM fuel type maps presented approximately 70% overall accuracy and 16% allocation disagreement. The McNemar's test indicated that the overall accuracy differences between the three produced fuel type maps were not significant ($p < 0.05$). Based on both overall and individual higher accuracies obtained with the use of the Quickbird image, this study suggests that the high spatial resolution might be more decisive than the high spectral resolution in Mediterranean fuel type mapping.

Keywords: SVMs; high spatial resolution; high spectral resolution; fuel type mapping; fire risk; fire impact; object-based; pixel-based

1. Introduction

Forest fires are an integral component of Mediterranean ecosystems since the Miocene. However, the second half of the past century presented a major change and regime shift [1]. This change in fire regime observed in recent decades in European Mediterranean [2–4] and elsewhere [5,6], is expressed by an increase of the number of fires and surface burnt [4,7,8], leading to more than 400,000 ha annually burnt areas in the EU Mediterranean region [1].

Given the spectacular increase in the number of wildland fires during the recent decades in the Euro-Mediterranean region, effective fire management strategies are needed to minimize fire hazard.

Efficient forest fire management requires an accurate knowledge of fuels at many spatial and temporal scales [9]. Fuels are defined as the physical characteristics, such as loading, size, and bulk density, of the live and dead biomass that contribute to the spread, intensity, and severity of wildland fire [10,11]. Based on knowledge of the spatial extent of the fuels, national authorities and fire managers can design fire prevention, detection, suppression and fire effects assessment strategies [12], such as the use and distribution of available fire-fighting resources, fuel treatment practices, fire towers and water tanks construction, trace gas emissions, and monitoring of vegetation recovery after fire [13]. In addition, accurate knowledge of forest fuel extent can be an effective component for mitigating the impacts of future wildfire on ecosystem services and restoring desirable structural attributes to fire suppressed forests as well as to infer ecosystem impacts of historically natural wildfires [14].

Remote sensing technology is capable of produce spatial estimations of fuel types and fuel loads, based on satellite systems of different spatial, temporal and spectral characteristics [9,15].

Most of the aforementioned studies relied on the use of broadband, medium spatial resolution imagery such as the Landsat TM and SPOT series, based on pixel-based classification approaches [16–18]. The value of imagery from the Advanced Spaceborne Thermal Emission and ReflectionRadiometer (ASTER) in fuel type and properties mapping has also been evaluated in conjunction with either pixel-based [19–21] or Geographic Object Based Image Analysis (GEOBIA) approaches [22,23].

Mediterranean forest areas are known for the high spatiotemporal heterogeneity of their vegetation patterns with respect to species composition and stand structure [24–27]. While this heterogeneity makes them aesthetically attractive, it hinders accurate mapping of forest-related parameters using applied remote sensing techniques [28,29]. Arroyo *et al.* [30], Gitas *et al.* [31] and Mallinis *et al.* [13] evaluated the use of multiscale object-based approaches with high spatial resolution imagery, in order to explore forest fuels delineation in Mediterranean areas. Moreover Lasaponara and Lanorte [32] employed a pixel-based approach with a Quickbird imagery to delineate fuel types according to the Prometheus fuel classification scheme.

However, very few studies have examined the possibility of hyperspectral data to overcome the limitations of traditional multispectral imagery [33–35]. Roberts *et al.* [34] evaluated data from the Earth Observing-1 (EO-1) Hyperion and AVIRIS sensors for mapping six land-cover classes in Santa

Barbara, California for fire danger assessment while Jia *et al.* [33] relied solely on AVIRIS data for assessing spatial patterns of forest fuel types in the Colorado Front Range. Lasaponara *et al.* [36] using airborne hyperspectral Multispectral Infrared and Visible Imaging Spectrometer (MIVIS) discriminated an adapted Prometheus fuel types scheme in Italy, using a conventional maximum likelihood classification. Finally, Keramitsoglou *et al.* [20] evaluated the use of EO-1 Hyperion satellite hyperspectral imagery near Athens, Greece for discriminating six fuel types.

While several recent studies have explored differences in information extraction efficacy between high-spatial resolution, multispectral and medium-spatial resolution hyperspectral imagery [37,38], none of them has focused on fuel type mapping purposes. Hence, when extracting forest related parameters, and particularly over complex forest areas, the issue regarding the choice of the most suitable spectral and spatial resolution for classification is of key importance [39].

Besides the exploration of spatial and spectral information exploitation, the remote sensing community investigates the use of various techniques and algorithms for extraction of useful information. Support vector machines (SVMs) are particularly appealing due to their ability to generalize well even with limited training samples, a common limitation for remote sensing applications [40]. SVMs have been used in remote sensing-based estimation and monitoring of biophysical parameters such as chlorophyll concentration, gross primary productivity, evapotranspiration, land/use land cover tasks, benthic habitat mapping using multi-beam sonar, forest mapping, burned area mapping, tree species detection using a variety of data sources ranging from VHR imagery to LIDAR datasets [9,40–44]. Comparative studies have also shown that classification by SVMs can be more accurate than popular contemporary techniques such as neural networks and decision trees as well as conventional probabilistic classifiers such as the maximum likelihood classification [45–48].

The main goal of our study is to evaluate and compare the potential of original spectral and spatial information of Quickbird, Landsat TM, and EO-1 Hyperion, joined with an SVMs classification approach, in discriminating Mediterranean fuel types on the same study site.

The specific objectives of this study included (1) fuel type mapping based on a Quickbird image using an object-based approach and SVMs classifier (2) generation of fuel type maps from Landsat-TM and EO-1 Hyperion imagery using a pixel-based approach and SVMs classifier and (3) assessment of the results and comparative evaluation of the potential of spatial against spectral resolution for fuel type mapping.

2. Materials and Methods

2.1. Outline of the Methodology

We evaluated and compared the fuel type maps generated upon the use of three satellite images with high/medium (*i.e.*, Quickbird), medium/high (*i.e.*, Landsat TM) and medium/very high (*i.e.*, EO-1 Hyperion), spatial/spectral resolution over the same Mediterranean site in northern Greece.

Pre-processing of the hyperspectral imagery included removal of non-calibrated and problematic bands, and a forward/backward Minimum Noise Fraction Transformation (MNFT) in order to separate the strong component of data noise (Figure 1).

Figure 1. Overall process diagram of this research study.

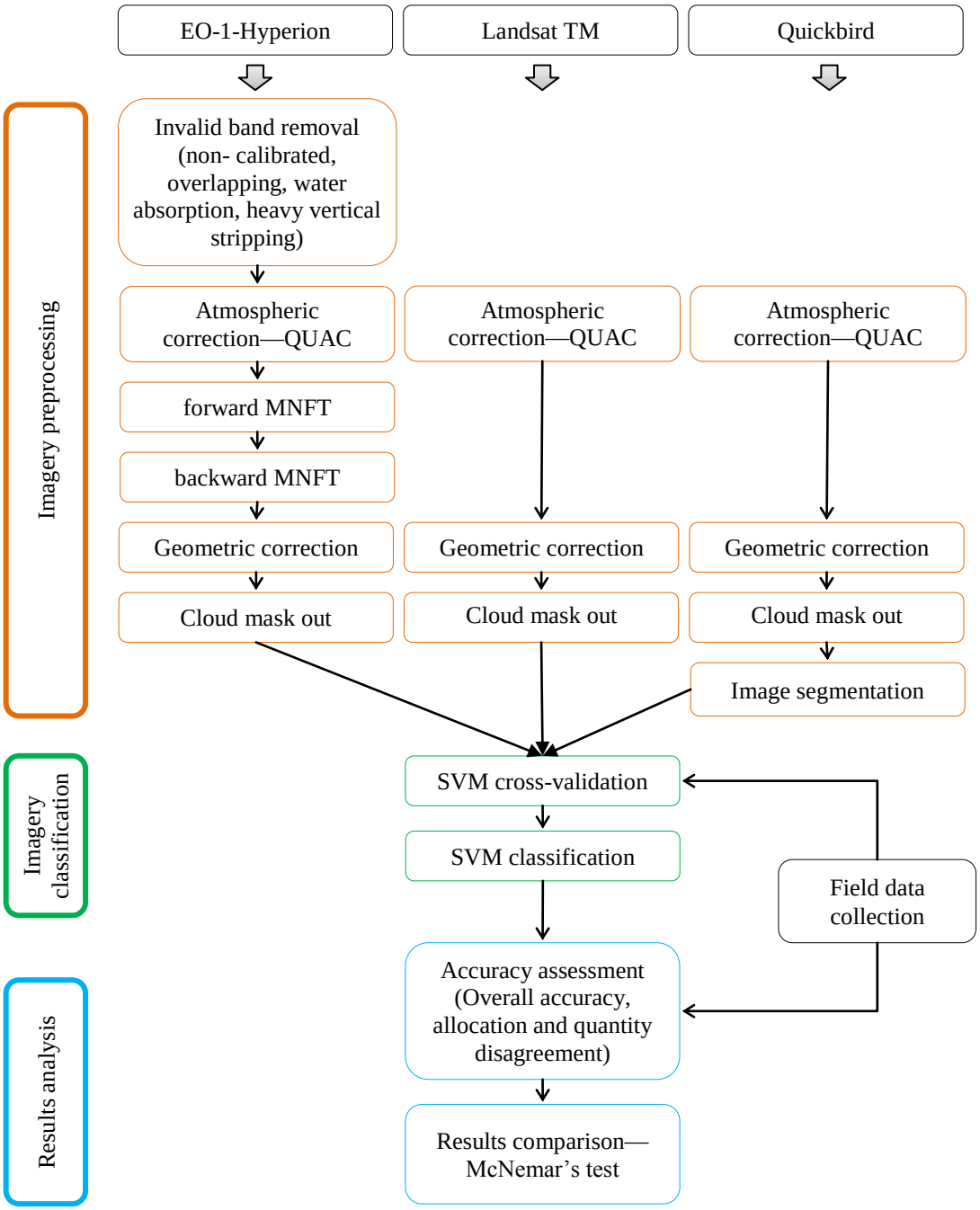

The multispectral images were also atmospherically corrected based on the same in-scene method used for the EO-1 Hyperion image. Finally, the EO-1 Hyperion and Landsat TM images were registered to the higher resolution Quickbird image which had been previously orthorectified using a rational function model and ground control points (GCPs) identified over existing VHR orthophotographs.

The three fuel maps were evaluated and relatively compared in terms of overall and individual class accuracies, allocation and quantity disagreement. Furthermore, statistically significant classification differences were assessed with the pairwise McNemar's test for dependent samples.

The same classification approach was applied to all data sets in order to obtain comparable results using the same coverage area, training sets and classification algorithm, (*i.e.*, SVMs). We used objects

as primary units of classification for the Quickbird imagery and pixels primary units for the Landsat and EO-1 Hyperion datasets. Imagery training samples were selected upon extensive field sampling and previous developed, site-specific fuel models. We did not considered any additional information such as image ratios (spectral indices), texture features, local contextual information or image-object form in the classification process.

2.2. Study Area

The University Forest of Taxiarchis is located on the southern and southwestern slopes of mount Cholomontas in Chalkidiki, in Central Macedonia region. It extends from 40 °23'E to 40 °28'E and 23 °28'N to 23 °34'N and covers an area of 60 km^2 (Figure 2). The University Forest area is also part of the NATURA2000 network (GR1270001-Oros Cholomontas).

Figure 2. Location of the study area, spatial extent of the EO-1 Hyperion, Quickbird, and Landsat TM imagery used in the research.

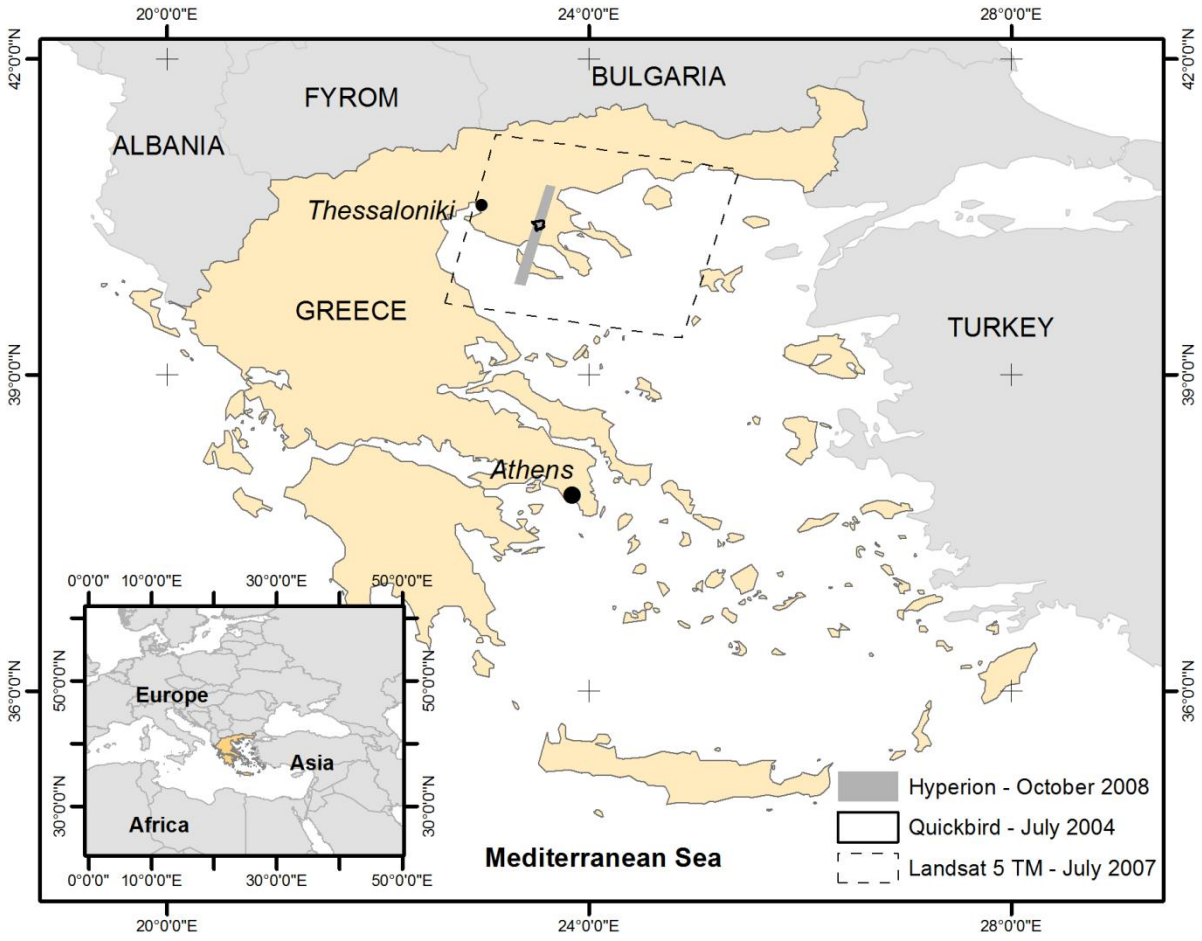

The terrain of the study area is diverse and very rough at places as a result of high difference in altitude, ranging between 320 and 1,200 m. The dense river network in conjunction with the sudden and intense rainfall during the winter period has formed gullies and has a wide affect in the region.

The Mediterranean climate of the area is characterized by short periods of drought, hot summers and mild winters. Main characteristic of the climate is the large fluctuations of rainfall during summer as well as the double dry season (July and September) with limited duration and intensity.

The study area forms a complex mosaic. Common forest species are Italian oak (*Quercus frainetto*), Black pine (*Pinus nigra*), Beech (*Fagus sylvatica*) and Norway spruce (*Pice aabies*). Gradually, mixed stands have formed as deciduous species invade the areas occupied by pines. Also, patches within the forest are covered with maquis (*Quercus ilex, Quercus coccifera, Erica arborea, etc.*), low herbaceous vegetation and scattered oak trees [28].

2.3. Satellite and Field Data

Imagery from the three spaceborne sensors used in this study present different spectral, spatial, and radiometric characteristics (Figure 3, Table 1).

Hyperion sensor on board the Earth Observing-1 (EO-1) mission is unique in that it collects high spectral resolution (0.1 μm) data spanning the VIS/NIR and SWIR wavelengths, with 220 contiguous spectral bands. Of these, 196 are well calibrated, but 24 bands are considered uncalibrated because they did not meet desired performance requirements or were noisy [49]. Hyperion is a push-broom instrument providing from a 705-km orbit, 30 m spatial resolution imagery over a 7.5-km-wide swath perpendicular to the satellite motion.

Figure 3. The EO-1 Hyperion (**a**); Quickbird (**b**); and Landsat TM (**c**) satellite images used in the study. In the lower row, respective subsets of the 3 images (**a1**–**c1**) on a larger scale illustrating spatial resolution differences.

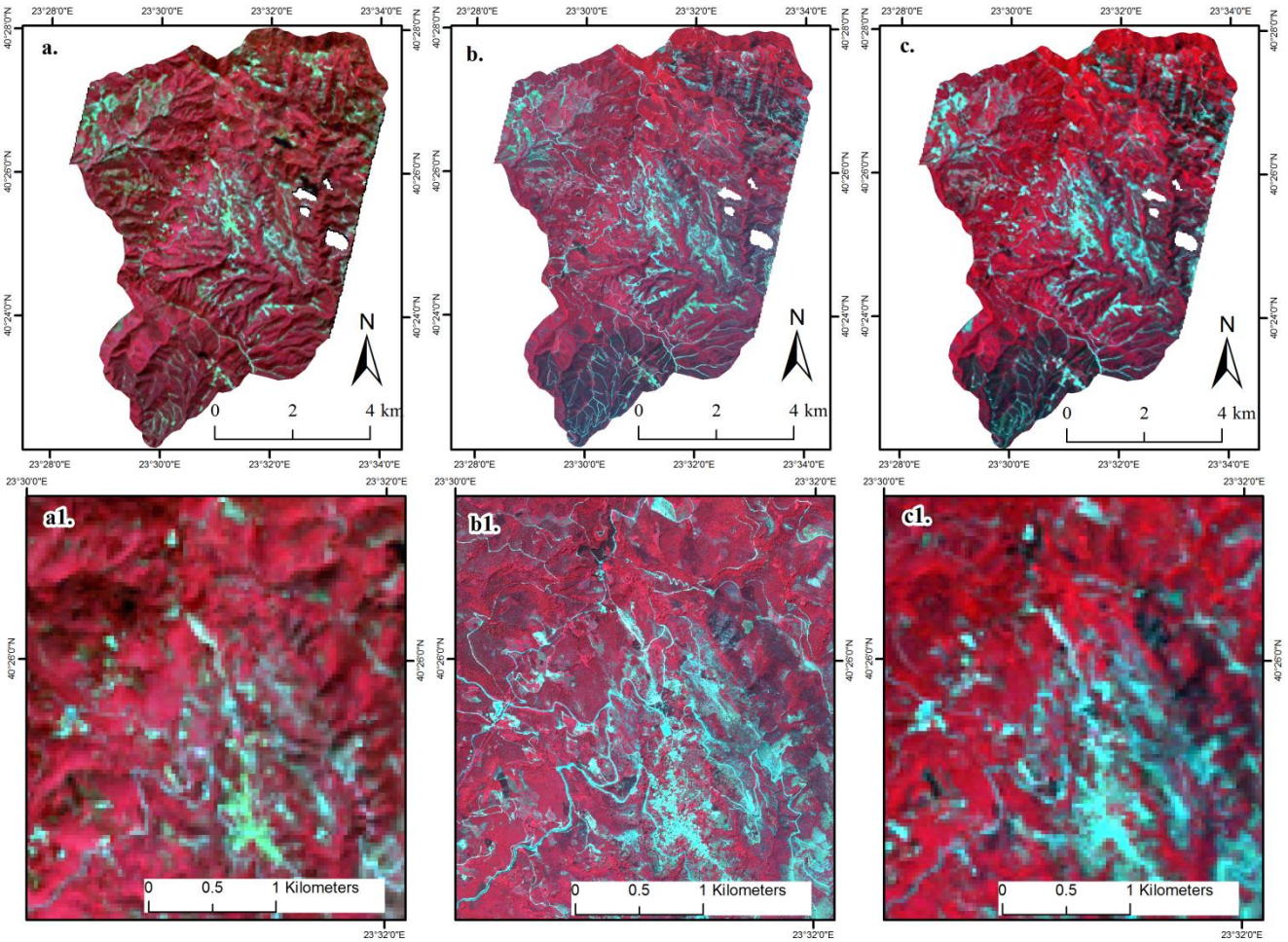

Table 1. Sensor and image specific characteristics of the data used in this study.

	EO-1 Hyperion	Quickbird	Landsat TM
Spectral range (/μm)	0.36–2.58	0.43–0.92	0.45–2.35
Spatial resolution (m)	30	2.4	30
Swath width (km)	7.7	16.5	185
Spectral resolution	0.1 μm	Variable	Variable
Signal-to-Noise Ratio (SNR)	150:1 to 50:1	166:1 to 172:1	72 to 60
Spectral coverage	Continuous	Discrete	Discrete
Radiometric resolution (bit)	12-bit	11-bit	8-bit
Number of bands (VNIR/SWIR)	196 (49/147)	4 (4/0)	6 (4/2)
Date of acquisition	October 2008	July 2004	July 2007
Sun elevation (deg.)	38.56	65.70	62.37

The Quickbird satellite acquires high-resolution push-broom imagery from a 450-km orbit. Quickbird multispectral images have 11-bit radiometric resolution and 2.4 and 0.6 spatial resolution at the multispectral (0.4–0.9 μm) and panchromatic (0.45–0.90 μm) mode respectively.

Finally, the Thematic Mapper (TM) onboard the Landsat-5 satellite was an across-track mechanical scanner. Landsat orbited the planet more than 150,000 times, transmitting over 2.5 million images of land surface conditions around the world. Thematic Mapper provided multispectral images of Earth's surface at an altitude of 705 km with 8-bit radiometric resolution and 30 m spatial resolution from 1984 to 2013 being the longest-operating Earth-observing satellite sensor in history. Quickbird and Landsat TM data were acquired on July 2004 and July 2007 respectively while the EO-1 Hyperion imagery was acquired on October 2008. A time interval of four years in the acquisition of the most recent and the oldest of the three images is noticed. However, the special protection status of the area (University forest, NATURA 2000 site) and the fact that no major fires or other disasters are recorded in the recent years certify the absence of changes within the specific period of this study.

Table 2. Fuel models of the study area.

Fuel Type	Fuel Model	Average Height (cm)	Total Fuel Load (t/ha)
f.t. 1	Evergreen-sclerophyllous shrublands (maquis) (up to 2 m)	152	28.9
f.t. 2	Litter layer of pine forests	4	3.1
f.t. 3	Litter layer of oak forests	6	5
f.t. 4	Litter layer of beech forests	4.5	4.7
f.t. 5	Litter layer of mixed forests	5	3.2
f.t. 6	Grassland	25	4.7

Reference data collected during an extensive field survey were used in the fuel models development and the later accuracy assessment of the produced maps. The study site was stratified based on vegetation maps, according to the dominant vegetation type. All strata were surveyed on site on mid-summer 2006, and 10 representative locations with typical ("average") fuel conditions per stratum were selected for the development of fuel models (Table 2) [13]. The study area was stratified for a second time, based on the existing fuel and vegetation maps, and revisited in August and October 2010 in order to sample homogenous field plots, suitable for the accuracy assessment, considering the

30 m spatial resolution of the imagery. It should be noted that during the October 2010 campaign a number of extra samples were collected to assist in the classification of grasslands in the EO-1 Hyperion image.

2.4. Image Pre-Processing

Pre-processing of the hyperspectral imagery is considered an essential step for enhancing classification accuracy and easing computational complexity. Significant efforts were devoted in the atmospheric correction and data reduction of the EO-1 Hyperion image, in order to address known problems of miscalibration and noise before use [50–52]. Initially, the original 242 bands were reduced to 123 bands, by excluding the bands: (1) being uncalibrated; (2) with very low SNR at both spectral ends (<430 nm and >2,400 nm); (3) being overlapping by the two spectrometers (VNIR and SWIR), and (4) with strong atmospheric water absorption features [33,53].

To minimize atmospheric effects and extract surface reflectance, the QUick Atmospheric Correction (QUAC) code was used for all three images [54]. QUAC code performs atmospheric correction on multi- and hyper-spectral imagery spanning all or part of the visible and near infrared–short wave infrared spectral range (0.4–2.5 μm) based on the empirical finding that the average reflectance of a collection of diverse material spectra is essentially scene-independent. QUAC utilizes an in-scene approach, requiring only approximate specification of sensor band locations and their radiometric calibration without any additional metadata [54]. The model performs appropriately when there are at least 10 diverse materials in the scene, as well as a sufficient number of dark pixels, in order to allow for a good estimation of the baseline spectrum.

Furthermore, we applied the forward-inverse Minimum Noise Fraction Transformation (MNFT) in the EO-1 Hyperion image, in order to reduce noise of the images for both the VNIR and SWIR bands of the image, for reducing the residual noise of the imagery [55]. The MNF components that resulted from the forward transformation were analyzed for their spectral information content based on their eigenvalues which represent the SNR. One part of the MNF components is associated with large eigenvalues and coherent eigenimages, and a complementary part is associated with near unity eigenvalues and noise-dominated images [56]. For the inverse MNF transformation solely the coherent eigenimages and more specifically eight components in the VNIR and five in the SWIR were used. The final EO-1 Hyperion dataset after the implementation of the inverse MNF transformation consisted of 123 bands. The Quickbird and Landsat TM images were also atmospherically corrected with the use of the QUAC code.

An orthorectification procedure was followed for the Quickbird image using a rational function model and 15 ground control points (GCPs) identified over existing VHR orthophotographs. Subsequently, the EO-1 Hyperion and Landsat TM images were registered to the higher resolution Quickbird image with an RMS error less than half a pixel (15 m).

Finally, the cloud mask generated based on the EO-1 Hyperion image was used to create a common reference extent boundary for the study site.

2.5. Image Segmentation

In the case of the VHR Quickbird image, image-objects were adopted as units of classification. Availability of high spatial resolution optical data in recent years and existence of a high resolution scene model (H-resolution) [57] for most applications, motivated a shift from the adoption of the pixel as a unit of classification to object-based classification methods [28]. This "high resolution" situation where pixels are significantly smaller than object, is predominantly attractive for exploiting the specific advantages of the GEOBIA approaches based on the definition of regions upon contiguous pixels belonging to the same class [58].

The segmentation algorithm applied in our work is a component of the multi-scale object-oriented fractal net evolution approach (FNEA) concept [59]. In this bottom-up segmentation technique, embedded within the commercial software Trimble eCognition Developer 8.7, individual pixels are perceived as the initial regions, which are sequentially merged pairwise into larger ones. The sequence of the merging objects, as well as the size and shape of the resulting objects, are empirically determined by the analyst [28]. The analyst specifies the layers of the image, as well as their importance, to be used for estimating spectral homogeneity/heterogeneity. The analyst, also, defines whether changes in the form of the objects resulting after the merge, will be considered in the heterogeneity estimate. The unitless scale parameter is determined to specify the maximum allowed increase in the heterogeneity after a pairwise merge of the objects [59]. For the Quickbird image scale parameter was set to 90, with shape and compactness equal to 0.1 and 0.5 respectively.

In order to compare the three fuel type maps, and classification of the Quickbird image was solely based on spectral information, disregarding local contextual information, image-object form and texture features that have been shown to improve classifications [28]. Pixel reference information collected in the field was transferred to the respective image objects.

2.6. Support Vector Machines Classification

SVMs is a supervised non-parametric statistical technique based on the structural risk minimization principle [60]. SVMs create a hyperplane through n-dimensional spectral-space that separates classes based on a user defined kernel function and parameters that are optimized using machine-learning to maximize the margin from the closest point to the hyperplane [44].

SVMs are particularly appealing in remote sensing works due to their ability to successfully analyze small training data sets, the ability to generalize to unseen data, the lack of any assumptions regarding the probability distribution of the data, and the balance achieved between accuracy attained on a given finite amount of training data [40].

However, due to the lack of any established heuristics for SVMs parameter selection, parameter assignment is a crucial issue that can significantly impact on the classification accuracy [40].

Selection of the optimal kernel and associated parameters can be difficult, though Gaussian radial basis function (RBF) has been proved effective in many classification problems for most land cover classes [44,61,62]. In the case of RBF, the γ parameter controlling the width of the Gaussian kernel is important since choosing a small value for the kernel width parameter may lead to over fitting, while large kernel width values may lead to over smoothing. In addition selection of a penalty parameter C

allows the SVMs to vary the degree of training data misclassified due to possible data error when optimizing the hyperplane, which is particularly important for non-separable training sets. The penalty parameter controls the trade-off between allowing training errors and forcing rigid margins with higher values of the parameter increasing the cost of misclassifying points and over fitting and lower values leading to under-fitting [63,64].

In order to selected the optimum *C* and gamma parameters of the RBF kernel for the three images we relied on a grid-search procedure based on a v-fold cross-validation procedure that estimates the generalization ability through repeatedly training SVMs [65]. For the EO-1 Hyperion image *C* and gamma were set to 100 and 0.5 respectively while for the Quickbird and Landsat TM images different parameters were used (*C* = 100, gamma = 0.5).

2.7. Accuracy Assessment

The vast majority of the reference samples for the accuracy assessment of the fuel type maps were located and sampled using GPS measurements and imagery print-outs during previous visits in the field during 2006 and 2010 [13,66]. Inaccessible points during field data collection were later identified using photo interpretation. For the accuracy evaluation of the Quickbird imagery, point reference information collected in the field was transferred to the respective image objects, which were then used for populating the confusion matrices.

The fuels maps were evaluated in terms of overall (OA) user's (UA) and producer's (PA) accuracies, allocation and quantity disagreement upon the three classification confusion matrices. Existence of statistically significant differences in classification accuracy, were assessed with the pairwise McNemar's test for dependent samples.

Allocation disagreement calculates the minimum of the proportion for each category omitted in the reference map and the proportion of the same category committed in the comparison map, multiplied by 2. Quantity disagreement measures the absolute differences in proportions difference between the reference map and a comparison map of the categories [67,68].

The statistical significance of differences between the overall accuracy of the fuel type maps, was assessed using the McNemar's test, Equation (1), considering that the testing sample set was common to all classifiers [69]. The test was applied for each of the three pairs of the fuel type maps.

$$\chi^2 = \frac{(f_{12} - f_{21})^2}{f_{12} + f_{21}} \quad (1)$$

in which f_{12}, f_{21} indicate agreement of only the one or the other map with the reference samples, respectively.

With this non-parametric test, the assessment is based on the evaluation of the derived χ^2 statistic and two classifications may be considered to be of different accuracy at the 95% level of confidence if $\chi^2 > 3.84$.

3. Results and Discussions

The fuel type maps produced from the implementation of the SVMs classification approach to the EO-1 Hyperion, Quickbird and Landsat TM images acquired over the Taxiarchis University Forest are depicted in Figure 4. The OA of the maps shows that all three classifications present satisfactory results in terms of overall performance and kappa coefficients. Quickbird classification with OA of 74.28% and a khat value of 0.70 over-performed the medium spatial resolution imagery classifications. Among the two medium spatial resolution datasets, the EO-1 Hyperion classification was slightly better (OA = 70%, khat = 0.65) in predicting the spatial distribution of fuel types in the area, compared to the classification result obtained from the Landsat TM which achieved an accuracy of 69.5% and khat of 0.64 (Table 3).

Figure 4. Fuel type classification obtained from the EO-1 Hyperion (**a**); Quickbird (**b**) and Landsat TM (**c**) data using the SVMs classification algorithm.

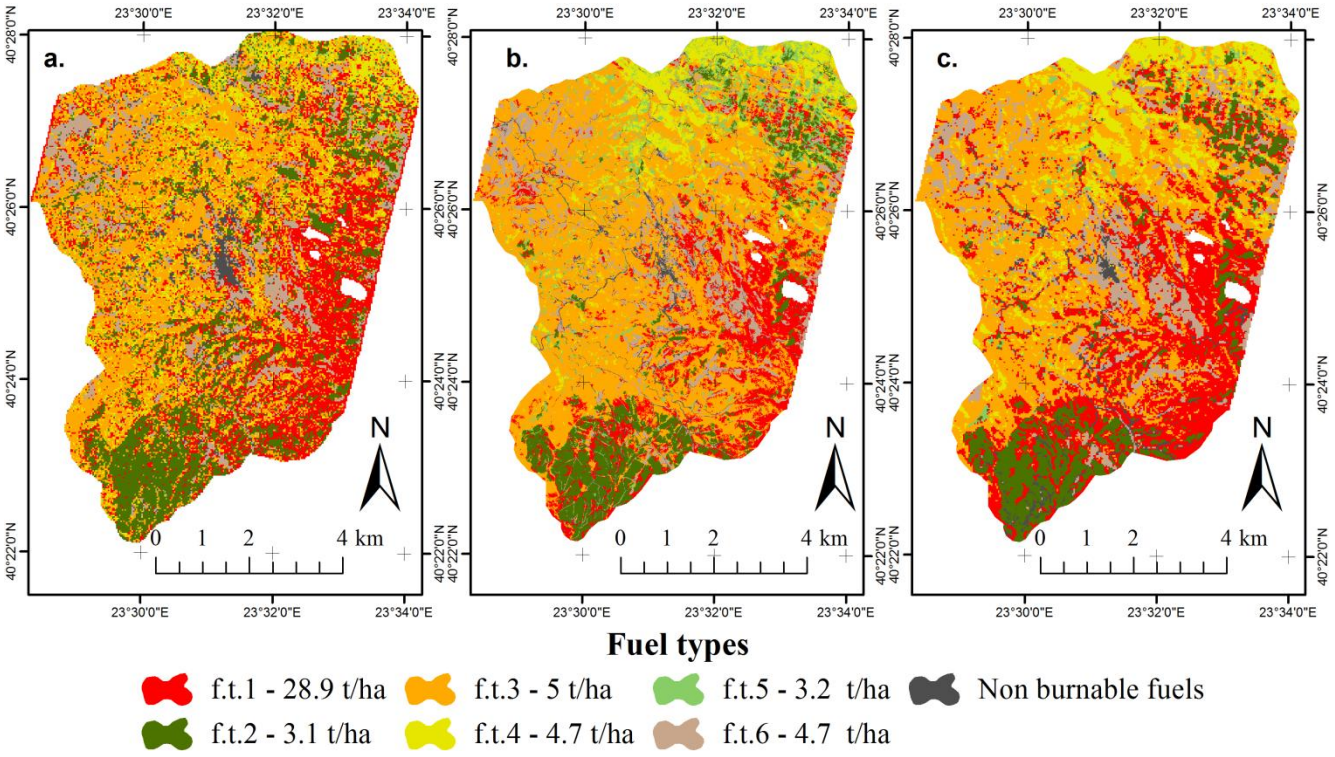

In terms of the individual classes' accuracy, in general different results were observed between the three datasets. Quickbird based fuel type classification presented not only higher overall accuracy but much more balanced commission/omission errors. A similar pattern in all three datasets is the underestimation of the f.t.5 (mixed forest) where ratio of omission over commission errors is above one. Especially in the case of the EO-1 Hyperion dataset omission errors are up to 7 times greater compared to the commissions errors.

Allocation disagreement values indicate incorrect spatial arrangement of the classified categories in comparison to the reference data (Figure 5) is the same for the two medium spatial resolution datasets (16%) and close to the allocation errors of the Quickbird imagery (17%). The quantity disagreement values expressing incorrect proportions of the various categories in comparison to the reference data is

more satisfactory for the Quickbird imagery (9%) compared to the quantity disagreement of EO-1 Hyperion (14%) and Landsat TM (15%) datasets.

Table 3. Error matrices of the three fuel classification approaches and accuracy assessment results based on overall, individual class accuracies and Khat values.

EO-1 Hyperion										
	Reference Data									
Classified Data	**f.t. 1**	**f.t.2**	**f.t.3**	**f.t.4**	**f.t.5**	**f.t.6**	**Non Fuels**	**Classified Totals**	**User Accuracy**	**Producer Accuracy**
f.t.1	33	3	4	8	8	3	8	67	49.25	84.62
f.t.2	2	45	2	1	8	2	2	62	72.58	80.36
f.t.3		3	51	1	5	3	3	66	77.27	72.86
f.t.4	4	2	10	51	9	4	3	83	61.45	78.46
f.t.5				1	8			9	88.89	20.51
f.t.6		3	3	3	1	48	2	64	80.00	78.69
NB fuel						1	29	30	96.67	61.7
Overall classification accuracy = 70.00							*Kappa coefficient = 0.65*			
Quickbird										
Classified Data	**f.t. 1**	**f.t.2**	**f.t.3**	**f.t.4**	**f.t.5**	**f.t.6**	**Non Fuels**	**Classified Totals**	**User Accuracy**	**Producer Accuracy**
f.t.1	25	4	5		4	3		41	60.98	64.1
f.t.2		45			4			49	91.84	78.69
f.t.3	12	5	57	14	7	6		101	56.44	91.49
f.t.4			5	46	8		1	60	76.67	70.77
f.t.5	1	2	1	4	16	1	1	26	61.54	41.03
f.t.6	1		2	1		48	2	54	88.89	81.43
NB fuel						3	43	46	93.48	80.36
Overall classification accuracy = 74.27							*Kappa coefficient = 0.70*			
Landsat TM										
Classified Data	**f.t. 1**	**f.t.2**	**f.t.3**	**f.t.4**	**f.t.5**	**f.t.6**	**Non Fuels**	**Classified Totals**	**User Accuracy**	**Producer Accuracy**
f.t.1	32	8	11	2	12	5	4	74	43.24	82.05
f.t.2	3	45			4	1		53	84.91	80.36
f.t.3	2	2	55	14	9	8		90	61.11	78.57
f.t.4			4	47	6	1		58	81.03	72.31
f.t.5	2	1		1	8			12	66.67	20.51
f.t.6				1		46	14	61	75.41	75.41
NB fuel							29	29	100.00	61.70
Reference Totals	39	56	70	65	39	61	47	377		
Overall classification accuracy = 69.50							*Kappa coefficient = 0.64*			

Figure 5. Quantity and allocation disagreement observed for the three fuel type maps, derived upon the EO-1 Hyperion, Quickbird and Landsat TM images.

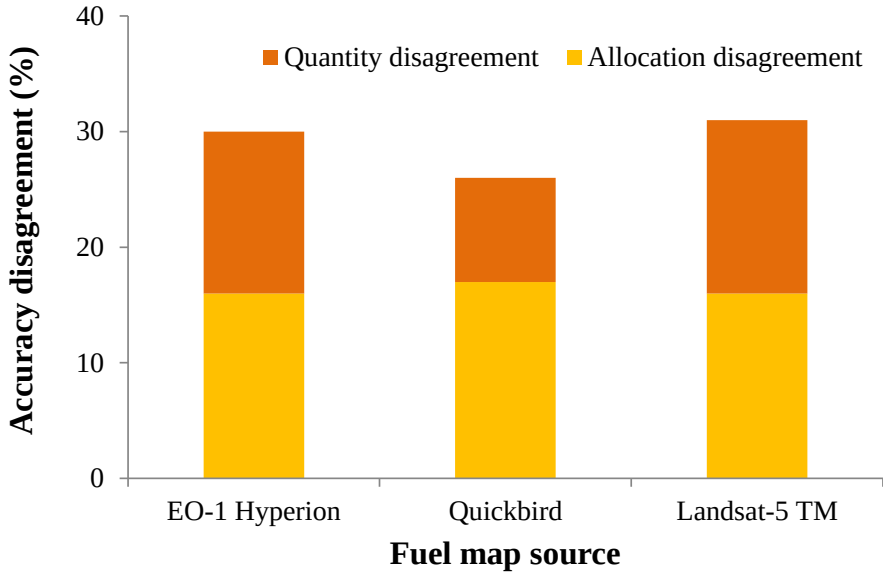

The high accurate labeling of pixels belonging to non-burnable fuel areas (NB fuel) in the EO-1 Hyperion dataset is reflected in the high ratio of omission/commission errors for this class. Large omission errors in this class are the same for the EO-1 Hyperion and TM datasets (38.3%) arising from the fact that this category includes objects such as roads, infrastructures *etc.*, having a width/size smaller than the 30 m spatial resolving capability of the sensors.

The largest discrepancies between omission and commission errors in both medium spatial resolution datasets (*i.e.*, Landsat TM and EO-1 Hyperion) are observed in f.t.5 (mixed forest) and f.t.1 (maquis) characterized by a spatial heterogeneous distribution pattern. Especially, patches of f.t.5 are found as relatively narrow transitional zones between homogeneous fuel type patches and hence they cannot always be detected by the relatively coarse resolution of the Hyperion and TM images. In the case of the Quickbird imagery discrepancies between omission and commission errors are more evident in f.t.3 (beech forest), where considering the homogeneity of these areas on the ground, should be attributed predominantly to the limited spectral information inherent in the image dataset. Moreover, the fact that EO-1 Hyperion and Landsat TM achieved similar accuracies in the discrimination of f.t.6 (grasslands) verifies the almost no-difference in the phenological state of grasslands observed between the mid-summer and October field surveys.

The findings of the McNemar's test indicated no statistically significant overall accuracy differences between the three produced fuel type maps (Table 4).

Table 4. McNemar's test indicated that there is no statistical difference in terms of accuracy between the three fuel type maps (statistically significant difference when $\chi^2 > 3.84$).

	EO-1Hyperion	**Landsat TM**
Landsat TM	0.11	
Quickbird	1.96	3.00

While airborne hyperspectral data has been extensively evaluated for assessing and mapping fuel types and properties either alone [33–36,70,71] or in combination with active remote sensing (LiDAR) [72,73], satellite hyperspectral datasets have not been thoroughly evaluated alone or in comparison to other datasets over the same task [20,34].

The higher accuracy achieved from the Quickbird image is in line with the results of Tanase and Gitas [23], who have also highlighted the effect of the spatial resolution in fuel type mapping classification accuracy. Specifically, the OA obtained from the classification of a Quickbird image was higher compared to the accuracy obtained for a slightly different fuel classification scheme from an ASTER VNIR image, processed also through GEOBIA analysis [23].

Regarding the importance of high spectral resolution in fuel type mapping, Keramitsoglou *et al.* [20], found that EO-1 Hyperion provided better classification accuracy exceeding 90%, compared to the 85% of an ASTER image. In another study, Roberts *et al.* [34] reported a better accuracy for AVIRIS relative to Hyperion as a result of the much lower SNR of Hyperion, the coarser spatial resolution, the spatial artifacts and the solar zenith angle of the scene. We also found that despite the high spectral resolution of EO-1 Hyperion and it's radiometric precision (12-bit) that is twice that of Quickbird imagery (11-bit), the later clearly outperformed the EO-1 Hyperion fuel type map in terms of classification accuracy. Our results are similar to Carter *et al.* [37], who compared the efficacy of Landsat-5 TM, Quickbird and EO-1 Hyperion data in discriminating invasive species populations and highlighted Quickbird superiority for the same objective.

Multispectral sensors data have known limitations such as sensor saturation and absence of specific narrowband to target and highlight specific biophysical and biochemical parameters [38,74–76]. We found almost similar accuracy for the medium spatial resolution sensors evaluated in the study regarding the high spectral resolution of EO-1 Hyperion. This is contrary to the findings of Keramitsoglou *et al.* [20] as described before but in line with the results obtained in other studies. For example, Gao and Liu [77] in a study for detection of land degradation found that Landsat-5 TM imagery outperformed the higher spectral resolution from the ASTER image producing higher overall and user's accuracies, concluding that the spectral resolution of an image is not as important as the information content of individual bands.

A number of recent studies have indicated the advantages of using discrete narrowband data from specific portions of the spectrum, rather than broadband data, to obtain the most sensitive quantitative or qualitative information on crop or vegetation characteristics [38].

A possible explanation might lie in the time of acquisition of the hyperspectral image, during mid-autumn, which might affect the SNR of the image. SNR may vary depending not only on sensor characteristics but also on the signal strength with summer images having a higher SNR than winter images, when the sun is at a lower zenith angle for the same time and place [78]. Specifically for the Hyperion images, previous research has identified almost a double SNR in summer compared to winter acquisitions [79].

With regards to the most accurate fuel type map of our study obtained from the Quickbird imagery, it is slightly less accurate compared to the results obtained from Lasaponara and Lanorte [32] over an area in South Italy who noted a 75.83% overall accuracy. Yet, in an earlier study of ours, over approximately the same area extent, image objects were assigned to respective fuel types using a CART statistical model with an overall accuracy over 80% [13]. This difference, and considering that

previous studies indicated the superiority of SVMs classifiers compared to CART algorithms [80], underlines the fact that an important component of the fuel type mapping process using VHR datasets is the use of object features that extend the original spectral and spatial information, such as image ratios, texture and contextual features. This is also verified by the finding that in the CART based fuel type map classification, half of the features selected corresponded either to textural measures after Haralick or to synthetic spectral bands. The higher accuracy achieved from the classification of the QB image is unquestionably related to the employment of GEOBIA. In relation, Blaschke [58] in a recent comprehensive review reports that a large number of studies have already verified that the existence of H-resolution scene model [81] significantly increases the within-class spectral variability and decreases the accuracy of pixel-based approaches when high and very-high resolution images are classified. In this work we employed different units of classification (one pixel *vs.* group of pixels) in order to avoid bias in the comparison resulting from the different scene and sensor characteristics. In fact, this work follows the suggestions of Blaschke [58] and Blasckhe *et al.* [82] according to which pixel-by-pixel techniques are more appropriate in the case of medium resolution imagery while—grouping of pixels into objects is needed in order to extract information from high spatial resolution sensors.

4. Conclusions

Accurate knowledge of the spatial extent of the fuels is of particular importance for national authorities and fire managers towards fire prevention, detection, fire effects assessment and impact quantification and mitigation strategies. Towards this direction we evaluated and compared three fuel type maps generated from EO-1 Hyperion, Quickbird and Landsat TM sensors over the same Mediterranean site.

This work can be perceived as the continuum of a research study conducted shortly before, over the same area, aiming at the evaluation of a Quickbird satellite imagery area for local scale fuel type mapping [13]. We are further motivated from the hypothesis that high spectral resolution may facilitate the identification of features while high spatial resolution may permit accurate location of features [83].

The overall accuracy of the Quickbird based fuel type map was higher than 74%, while the EO-1 Hyperion and Landsat TM based fuel type maps were of similar accuracy, around 70%. The McNemar's test indicated no statistically significant overall accuracy differences between the three produced fuel type maps. Between the medium spatial resolution images that were used in this study and provided similar results, EO-1 Hyperion, though its larger number of spectral bands should improve mapping, has also higher data cost and considerable more complicated preprocessing phase due to increased data volume and inherent noise, in contrast to Landsat TM imagery which is easier to process, and covers a larger area. Implicit assumptions of the greater utility of high resolution satellite imagery are widespread, but do not always hold true [37], depending not only in the classification content, but on image acquisition parameters and scene configuration.

Classification results are related to several factors besides sensor characteristics and extrapolation of our findings to other areas or biomes require further studies. Future research will advance the use of the high spatial and high spectral data for fuel type mapping within the framework of data fusion in order to take advantage of the spectral and spatial resolution of each data source. The improved

spectral, radiometric and SNR of the Operational Land Imager (OLI) on board the Landsat Data Continuity Mission (LDCM) and the 8-band WorldView-2 sensor is a further promising data source that should be evaluated for fuel type mapping purposes over Mediterranean areas.

Acknowledgments

This research has received funding by the European Union (European Social Fund-ESF) and Greek national funds through the Operational Program "Education and Lifelong Learning" of the National Strategic Reference Framework (NSRF) Research Funding Program: THALES. Investing in knowledge society through the European Social Fund.

EO-1 Hyperion and Landsat-5TM data used were available at no-cost from the US Geological Survey.

We would like to thank the 3 anonymous reviewers whose insightful comments helped to substantially improve this manuscript.

Author Contributions

Giorgos Mallinis proposed and developed the research design, performed the image segmentation and SVM classification analysis, manuscript writing, results interpretation and coordinated the revision activities. Georgia Galidaki performed the hyperspectral image preprocessing, contributed to the classification and accuracy assessment and contributed to the manuscript writing and revision. Ioannis Gitas contributed to optical image processing, discussion writing and manuscript revision.

Conflicts of Interest

The authors declare no conflict of interest.

References

1. San-Miguel-Ayanz, J.; Moreno, J.M.; Camia, A. Analysis of large fires in European Mediterranean landscapes: Lessons learned and perspectives. *For. Ecol. Manag.* **2014**, *294*, 11–22.
2. Pausas, J.G.; Vallejo, R.V. The Role of Fire in European Mediterranean Ecosystems. In *Remote Sensing of Large Wildfires*; Chuvieco, E., Ed.; Springer: Berlin/Heidelberg, Germany, 1999; pp. 3–16.
3. Piñol, J.; Terradas, J.; Lloret, F. Climate warming, wildfire hazard, and wildfire occurrence in coastal eastern Spain. *Clim. Chang.* **1998**, *38*, 345–357.
4. Koutsias, N.; Xanthopoulos, G.; Founda, D.; Xystrakis, F.; Nioti, F.; Pleniou, M.; Mallinis, G.; Arianoutsou, M. On the relationships between forest fires and weather conditions in Greece from long-term national observations (1894–2010). *Int. J. Wildland Fire* **2013**, *22*, 493–507.
5. Kasischke, E.S.; Hyer, E.J.; Novelli, P.C.; Bruhwiler, L.P.; French, N.H.F.; Sukhinin, A.I.; Hewson, J.H.; Stocks, B.J. Influences of boreal fire emissions on Northern Hemisphere atmospheric carbon and carbon monoxide. *Glob. Biogeochem. Cycl.* **2005**, *19*, 1–16.
6. Flannigan, M.D.; Krawchuk, M.A.; de Groot, W.J.; Wotton, B.M.; Gowman, L.M. Implications of changing climate for global wildland fire. *Int. J. Wildland Fire* **2009**, *18*, 483–507.

7. Dimitrakopoulos, A.P.; Vlahou, M.; Anagnostopoulou, C.G.; Mitsopoulos, I.D. Impact of drought on wildland fires in Greece: Implications of climatic change? *Clim. Chang.* **2011**, *109*, 331–347.
8. Pausas, J.G.; Fernández-Muñoz, S. Fire regime changes in the Western Mediterranean Basin: From fuel-limited to drought-driven fire regime. *Clim. Chang.* **2012**, *110*, 215–226.
9. Keane, R.E.; Burgan, R.; van Wagtendonk, J. Mapping wildland fuels for fire management across multiple scales: Integrating remote sensing, GIS, and biophysical modeling. *Int. J. Wildland Fire* **2001**, *10*, 301–319.
10. Anderson, H.E. *Aids to Determining Fuel Models for Estimating Fire Behavior*; U.S. Department of Agriculture, Forest Service, Intermountain Forest and Range Experiment Station: Ogden, UT, USA, 1982.
11. Burgan, R.E.; Rothermel, R.C. *BEHAVE: Fire Behavior Prediction and Fuel Modeling System—FUEL Subsystem*; U.S. Department of Agriculture, Forest Service, Intermountain Research Station: Ogden, UT, USA, 1984.
12. Chuvieco, E.; Riaño, D.; van Wagtendok, J.; Morsdof, F. Fuel Loads and Fuel Type Mapping. In *Wildland Fire Danger Estimation and Mapping*; Chuvieco, E., Ed.; World Scientific Publishing: Singapore, 2003; pp. 119–142.
13. Mallinis, G.; Mitsopoulos, I.D.; Dimitrakopoulos, A.P.; Gitas, I.Z.; Karteris, M. Local-scale fuel-type mapping and fire behavior prediction by employing high-resolution satellite imagery. *IEEE J. Sel. Top. Appl. Earth Obs. Remote Sens.* **2008**, *1*, 230–239.
14. Campbell, J.L.; Ager, A.A. Forest wildfire, fuel reduction treatments, and landscape carbon stocks: A sensitivity analysis. *J. Environ. Manag.* **2013**, *121*, 124–132.
15. Arroyo, L.A.; Pascual, C.; Manzanera, J.A. Fire models and methods to map fuel types: The role of remote sensing. *For. Ecol. Manag.* **2008**, *256*, 1239–1252.
16. Lentile, L.B.; Smith, A.M.S.; Hudak, A.T.; Morgan, P.; Bobbitt, M.J.; Lewis, S.A.; Robichaud, P.R. Remote sensing for prediction of 1-year post-fire ecosystem condition. *Int. J. Wildland Fire* **2009**, *18*, 594–608.
17. Chuvieco, E.; Salas, J. Mapping the spatial distribution of forest fire danger using GIS. *Int. J. Geogr. Inf. Syst.* **1996**, *10*, 333–345.
18. Koutsias, N.; Karteris, M. Classification analyses of vegetation for delineating forest fire fuel complexes in a Mediterranean test site using satellite remote sensing and GIS. *Int. J. Remote Sens.* **2003**, *24*, 3093–3104.
19. Falkowski, M.J.; Gessler, P.E.; Morgan, P.; Hudak, A.T.; Smith, A.M.S. Characterizing and mapping forest fire fuels using ASTER imagery and gradient modeling. *For. Ecol. Manag.* **2005**, *217*, 129–146.
20. Keramitsoglou, I.; Kontoes, C.; Sykioti, O.; Sifakis, N.; Xofis, P. Reliable, accurate and timely forest mapping for wildfire management using ASTER and Hyperion satellite imagery. *For. Ecol. Manag.* **2008**, *255*, 3556–3562.
21. Lasaponara, R.; Lanorte, A. Remotely sensed characterization of forest fuel types by using satellite ASTER data. *Int. J. Appl. Earth Obs. Geoinf.* **2007**, *9*, 225–234.
22. Alonso-Benito, A.; Arroyo, L.A.; Arbelo, M.; Hernández-Leal, P.; González-Calvo, A. Pixel and object-based classification approaches for mapping forest fuel types in Tenerife Island from ASTER data. *Int. J. Wildland Fire* **2013**, *22*, 306–317.

23. Tanase, M.A.; Gitas, I.Z. An examination of the effects of spatial resolution and image analysis technique on indirect fuel mapping. *IEEE J. Sel. Top. Appl. Earth Obs. Remote Sens.* **2008**, *1*, 220–229.
24. Shoshany, M. Satellite remote sensing of natural Mediterranean vegetation: A review within an ecological context. *Prog. Phys. Geogr.* **2000**, *24*, 153–178.
25. Scarascia-Mugnozza, G.; Oswald, H.; Piussi, P.; Radoglou, K. Forests of the Mediterranean region: Gaps in knowledge and research needs. *For. Ecol. Manag.* **2000**, *132*, 97–109.
26. Ozdemir, I.; Karnieli, A. Predicting forest structural parameters using the image texture derived from worldview-2 multispectral imagery in a dryland forest, Israel. *Int. J. Appl. Earth Obs. Geoinf.* **2011**, *13*, 701–710.
27. Mallinis, G.; Koutsias, N.; Makras, A.; Karteris, M. Forest parameters estimation in a European Mediterranean landscape using remotely sensed data. *For. Sci.* **2004**, *50*, 450–460.
28. Mallinis, G.; Koutsias, N.; Tsakiri-Strati, M.; Karteris, M. Object-based classification using Quickbird imagery for delineating forest vegetation polygons in a Mediterranean test site. *ISPRS J. Photogramm. Remote Sens.* **2008**, *63*, 237–250.
29. Mallinis, G.; Mitsopoulos, I.; Stournara, P.; Patias, P.; Dimitrakopoulos, A. Canopy fuel load mapping of Mediterranean pine sites based on individual tree-crown delineation. *Remote Sens.* **2013**, *5*, 6461–6480.
30. Arroyo, L.A.; Healey, S.P.; Cohen, W.B.; Cocero, D.; Manzanera, J.A. Using object-oriented classification and high-resolution imagery to map fuel types in a Mediterranean region. *J. Geophys. Res. Biogeosci.* **2006**, *111*, doi:10.1029/2005JG000120.
31. Gitas, I.Z.; Mitri, G.H.; Kazakis, G.; Ghosn, D.; Xanthopoulos, G. Fuel type mapping in Anopolis, Crete by employing QuickBird imagery and object-based classification. *For. Ecol. Manag.* **2006**, *234*, S228.
32. Lasaponara, R.; Lanorte, A. On the capability of satellite VHR QuickBird data for fuel type characterization in fragmented landscape. *Ecol. Model.* **2007**, *204*, 79–84.
33. Jia, G.J.; Burke, I.C.; Goetz, A.F.H.; Kaufmann, M.R.; Kindel, B.C. Assessing spatial patterns of forest fuel using AVIRIS data. *Remote Sens. Environ.* **2006**, *102*, 318–327.
34. Roberts, D.A.; Dennison, P.E.; Gardner, M.E.; Hetzel, Y.; Ustin, S.L.; Lee, C.T. Evaluation of the potential of Hyperion for fire danger assessment by comparison to the Airborne Visible/Infrared Imaging Spectrometer. *IEEE Trans. Geosci. Remote Sens.* **2003**, *41*, 1297–1310.
35. Roberts, D.A.; Dennison, P.E.; Peterson, S.; Sweeney, S.; Rechel, J. Evaluation of Airborne Visible/Infrared Imaging Spectrometer (AVIRIS) and Moderate Resolution Imaging Spectrometer (MODIS) measures of live fuel moisture and fuel condition in a shrubland ecosystem in southern California. *J. Geophys. Res.: Biogeosci.* **2006**, *111*, doi:10.1029/2005JG000113.
36. Lasaponara, R.; Lanorte, A.; Pignatti, S. Characterization and mapping of fuel types for the Mediterranean ecosystems of Pollino National Park in southern Italy by using hyperspectral MIVIS data. *Earth Interact.* **2006**, *10*, 1–11.
37. Carter, G.A.; Lucas, K.L.; Blossom, G.A.; Holiday, C.L.L.; Mooneyhan, D.S.; Fastring, D.R.; Holcombe, T.R.; Griffith, J.A. Remote sensing and mapping of tamarisk along the Colorado river, USA: A comparative use of summer-acquired Hyperion, thematic mapper and Quickbird data. *Remote Sens.* **2009**, *1*, 318–329.

38. Thenkabail, P.S.; Enclona, E.A.; Ashton, M.S.; Legg, C.; de Dieu, M.J. Hyperion, IKONOS, ALI, and ETM+ sensors in the study of African rainforests. *Remote Sens. Environ.* **2004**, *90*, 23–43.
39. Dalponte, M.; Bruzzone, L.; Vescovo, L.; Gianelle, D. The role of spectral resolution and classifier complexity in the analysis of hyperspectral images of forest areas. *Remote Sens. Environ.* **2009**, *113*, 2345–2355.
40. Mountrakis, G.; Im, J.; Ogole, C. Support vector machines in remote sensing: A review. *ISPRS J. Photogramm. Remote Sens.* **2011**, *66*, 247–259.
41. Hasan, R.C.; Ierodiaconou, D.; Monk, J. Evaluation of four supervised learning methods for benthic habitat mapping using backscatter from multi-beam sonar. *Remote Sens.* **2012**, *4*, 3427–3443.
42. Vaughn, N.R.; Moskal, L.M.; Turnblom, E.C. Tree species detection accuracies using discrete point lidar and airborne waveform lidar. *Remote Sens.* **2012**, *4*, 377–403.
43. Mirik, M.; Ansley, R.J.; Steddom, K.; Jones, D.C.; Rush, C.M.; Michels, G.J., Jr.; Elliott, N.C. Remote distinction of a noxious weed (Musk Thistle: Carduus Nutans) using airborne hyperspectral imagery and the support vector machine classifier. *Remote Sens.* **2013**, *5*, 612–630.
44. Heumann, B.W. An object-based classification of mangroves using a hybrid decision tree-support vector machine approach. *Remote Sens.* **2011**, *3*, 2440–2460.
45. Dalponte, M.; Ørka, H.O.; Gobakken, T.; Gianelle, D.; Næsset, E. Tree species classification in boreal forests with hyperspectral data. *IEEE Trans. Geosci. Remote Sens.* **2013**, *51*, 2632–2645.
46. Feret, J.B.; Asner, G.P. Tree species discrimination in tropical forests using airborne imaging spectroscopy. *IEEE Trans. Geosci. Remote Sens.* **2013**, *51*, 73–84.
47. Melgani, F.; Bruzzone, L. Classification of hyperspectral remote sensing images with support vector machines. *IEEE Trans. Geosci. Remote Sens.* **2004**, *42*, 1778–1790.
48. Pal, M.; Mather, P.M. Assessment of the effectiveness of support vector machines for hyperspectral data. *Future Gener. Comput. Syst.* **2004**, *20*, 1215–1225.
49. Middleton, E.M.; Ungar, S.G.; Mandl, D.J.; Ong, L.; Frye, S.W.; Campbell, P.E.; Landis, D.R.; Young, J.P.; Pollack, N.H. The earth observing one (EO-1) satellite mission: Over a decade in space. *IEEE J. Sel. Top. Appl. Earth Obs. Remote Sens.* **2013**, *6*, 243–256.
50. Datt, B.; McVicar, T.R.; van Niel, T.G.; Jupp, D.L.B.; Pearlman, J.S. Preprocessing EO-1 Hyperion hyperspectral data to support the application of agricultural indexes. *IEEE Trans. Geosci. Remote Sens.* **2003**, *41*, 1246–1259.
51. Goodenough, D.G.; Dyk, A.; Niemann, K.O.; Pearlman, J.S.; Chen, H.; Han, T.; Murdoch, M.; West, C. Processing Hyperion and ALI for forest classification. *IEEE Trans. Geosci. Remote Sens.* **2003**, *41*, 1321–1331.
52. Pengra, B.W.; Johnston, C.A.; Loveland, T.R. Mapping an invasive plant, Phragmites australis, in coastal wetlands using the EO-1 Hyperion hyperspectral sensor. *Remote Sens. Environ.* **2007**, *108*, 74–81.
53. Pu, R.; Gong, P.; Yu, Q. Comparative analysis of EO-1 ALI and Hyperion, and Landsat ETM+ data for mapping forest crown closure and leaf area index. *Sensors* **2008**, *8*, 3744–3766.
54. Bernstein, L.S.; Jin, X.; Gregor, B.; Adler-Golden, S.M. Quick atmospheric correction code: Algorithm description and recent upgrades. *Opt. Eng.* **2012**, *51*, doi:10.1117/1.OE.51.11.111719.

55. Gersman, R.; Ben-Dor, E.; Beyth, M.; Avigad, D.; Abraha, M.; Kibreab, A. Mapping of hydrothermally altered rocks by the EO-1 Hyperion sensor, Northern Danakil Depression, Eritrea. *Int. J. Remote Sens.* **2008**, *29*, 3911–3936.
56. Hsu, S.M.; Burke, H.H.K.; Orloff, S.; Griffin, M. Examples of EO-1 Data Analysis. In Proceedings of the Algorithms and Technologies for Multispectral, Hyperspectral, and Ultraspectral Imagery IX, Orlando, FL, USA, 24 September 2003; pp. 362–372.
57. Hay, G.J.; Niemann, K.O.; McLean, G.F. An object-specific image-texture analysis of H-resolution forest imagery. *Remote Sens. Environ.* **1996**, *55*, 108–122.
58. Blaschke, T. Object based image analysis for remote sensing. *ISPRS J. Photogramm. Remote Sens.* **2010**, *65*, 2–16.
59. Benz, U.C.; Hofmann, P.; Willhauck, G.; Lingenfelder, I.; Heynen, M. Multi-resolution, object-oriented fuzzy analysis of remote sensing data for GIS-ready information. *ISPRS J. Photogramm. Remote Sens.* **2004**, *58*, 239–258.
60. Vapnik, V.N. *The Nature of Statistical Learning Theory*, 2nd ed.; Springer: New York, NY, USA, 2000; p. 314.
61. Zhang, J.; Lin, X.; Ning, X. SVM-based classification of segmented airborne LiDAR point clouds in urban areas. *Remote Sens.* **2013**, *5*, 3749–3775.
62. Yang, X. Parameterizing support vector machines for land cover classification. *Photogramm. Eng. Remote Sens.* **2011**, *77*, 27–38.
63. Jebur, M.N.; Mohd Shafri, H.Z.; Pradhan, B.; Tehrany, M.S. Per-pixel and object-oriented classification methods for mapping urban land cover extraction using SPOT 5 imagery. *Geocarto Int.* **2013**, doi:10.1080/10106049.2013.848944.
64. Alpaydin, E. *Introduction to Machine Learning*; MIT Press: Cambridge, MA, USA, 2004; p. 415.
65. Chang, C.-C.; Lin, C.-J. LIBSVM: A library for support vector machines. *ACM Trans. Intell. Syst. Technol.* **2011**, *2*, 1–27.
66. Galidaki, G.; Gitas, I.Z. Mediterranean forest species mapping using classification of Hyperion imagery. *Geocarto Int.* **2013**, in press.
67. Pontius, R.G.; Millones, M. Death to Kappa: Birth of quantity disagreement and allocation disagreement for accuracy assessment. *Int. J. Remote Sens.* **2011**, *32*, 4407–4429.
68. Daniel, G.; Gregory, S.B.; Javier, M. Accuracy Assessment for Soft Classification Maps. In *Remote Sensing of Natural Resources*; CRC Press: Boca Raton, FL, USA, 2013; pp. 57–86.
69. Foody, G.M. Thematic map comparison: Evaluating the statistical significance of differences in classification accuracy. *Photogramm. Eng. Remote Sens.* **2004**, *70*, 627–633.
70. Jia, G.J.; Burke, I.C.; Kaufmann, M.R.; Goetz, A.F.H.; Kindel, B.C.; Pu, Y. Estimates of forest canopy fuel attributes using hyperspectral data. *For. Ecol. Manag.* **2006**, *229*, 27–38.
71. Lasaponara, R.; Lanorte, A.; Pignatti, S. Multiscale fuel type mapping in fragmented ecosystems: Preliminary results from hyperspectral MIVIS and multispectral Landsat TM data. *Int. J. Remote Sens.* **2006**, *27*, 587–593.
72. Koetz, B.; Morsdorf, F.; van der Linden, S.; Curt, T.; Allgöwer, B. Multi-source land cover classification for forest fire management based on imaging spectrometry and LiDAR data. *For. Ecol. Manag.* **2008**, *256*, 263–271.

73. Varga, T.A.; Asner, G.P. Hyperspectral and LiDAR remote sensing of fire fuels in Hawaii volcanoes National Park. *Ecol. Appl.* **2008**, *18*, 613–623.
74. Thenkabail, P.S.; Enclona, E.A.; Ashton, M.S.; van der Meer, B. Accuracy assessments of hyperspectral waveband performance for vegetation analysis applications. *Remote Sens. Environ.* **2004**, *91*, 354–376.
75. Gitelson, A.A.; Gritz, Y.; Merzlyak, M.N. Relationships between leaf chlorophyll content and spectral reflectance and algorithms for non-destructive chlorophyll assessment in higher plant leaves. *J. Plant Physiol.* **2003**, *160*, 271–282.
76. Mariotto, I.; Thenkabail, P.S.; Huete, A.; Slonecker, E.T.; Platonov, A. Hyperspectral *versus* multispectral crop-productivity modeling and type discrimination for the HyspIRI mission. *Remote Sens. Environ.* **2013**, *139*, 291–305.
77. Gao, J.; Liu, Y. Mapping of land degradation from space: A comparative study of Landsat ETM + and ASTER data. *Int. J. Remote Sens.* **2008**, *29*, 4029–4043.
78. Platt, R.V.; Goetz, A.F.H. A comparison of AVIRIS and Landsat for land use classification at the urban fringe. *Photogramm. Eng. Remote Sens.* **2004**, *70*, 813–819.
79. Kruse, F.A.; Boardman, J.W.; Huntington, J.F. Comparison of airborne hyperspectral data and EO-1 Hyperion for mineral mapping. *IEEE Trans. Geosci. Remote Sens.* **2003**, *41*, 1388–1400.
80. Shao, Y.; Lunetta, R.S. Comparison of support vector machine, neural network, and CART algorithms for the land-cover classification using limited training data points. *ISPRS J. Photogramm. Remote Sens.* **2012**, *70*, 78–87.
81. Strahler, A.H.; Woodcock, C.E.; Smith, J.A. On the nature of models in remote sensing. *Remote Sens. Environ.* **1986**, *20*, 121–139.
82. Blaschke, T.; Hay, G.J.; Kelly, M.; Lang, S.; Hofmann, P.; Addink, E.; Queiroz Feitosa, R.; van der Meer, F.; van der Werff, H.; van Coillie, F.; *et al.* Geographic object-based image analysis—Towards a new paradigm. *ISPRS J. Photogramm. Remote Sens.* **2014**, *87*, 180–191.
83. Gross, H.N.; Schott, J.R. Application of spectral mixture analysis and image fusion techniques for image sharpening. *Remote Sens. Environ.* **1998**, *63*, 85–94.